CFD simulations of the effect of dust diameter on the dispersion in the 1 m³ explosion vessel

Maria Portarapillo[a]*, Marco Trofa[a], Roberto Sanchirico[b], Almerinda Di Benedetto[a]

[a] Dipartimento di Ingegneria Chimica, dei Materiali e della Produzione Industriale, Università degli Studi di Napoli Federico II, Piazzale V. Tecchio 80, 80125, Napoli, Italy

[c] Istituto di Ricerche sulla Combustione, Consiglio Nazionale delle Ricerche (CNR), Piazzale V. Tecchio 80, 80125, Napoli, Italy

maria.portarapillo@unina.it

There are at least two main requirements for repeatable and reliable measurements of flammability and explosibility parameters of dusts: a uniform dispersion of solid particles inside the test vessel and a homogeneous degree of turbulence. Measurements of these parameters are performed in spherical vessels (20 L sphere or 1 m³ sphere). In several literature works, it has been shown that, in the standard 20 L sphere, the dust injection system generates a non-uniform dust cloud, while high gradients characterize the turbulent flow field. In our recent work, CFD simulations of flow field and dust concentration distribution in the 1 m³ spherical vessel were carried out and the results compared to the data previously obtained for the 20 L. It has been found that in the 1 m³ vessel, the spatial distribution of the turbulent kinetic energy is lower and much more uniform. Concerning the dust distribution, as in the case of the 20 L, dust is mainly concentrated at the outer zones of the vortices generated inside the vessel. In this work we use the previously validated CFD model to simulate the dust dispersion inside the 1 m³ vessel at different dust diameters. Results show that on increasing the dust diameter, the dust paths are different from those of the fluid flow until the sedimentation effect prevails and the turbulence field becomes similar to the dust-free air case. Since the spatial distribution of the turbulent kinetic energy is lower and much more uniform than in the 20 L sphere, the 1 m³ vessel is less susceptible to variations in the dust intrinsic properties, making parameter measurements more reliable and repeatable.

1. Introduction

Dusts or dust-like substances are processed or are by-products of the production process in many industries. In both cases, a large majority of dust-like substances pose the danger of fire or possibly even explosions. Eighty percent of all industrial dusts are combustible and even a dust layer of 1 mm in a closed room is sufficient to trigger an explosion (or magnify an occurring one, i.e., secondary explosion) when the dust is swirled up and ignited. Moreover, most industries possibly affected by dust explosions are not sufficiently aware of the danger (in contrast to the danger of gas explosions), underlining the importance of prevention and mitigation/protection. In order to characterize the sensitivity and the severity of explosion in case of ignition, each handled dust requires the explosibility and flammability parameters assessment. Most of these parameters (minimum explosible concentration, MEC; limiting oxygen concentration, LOC; maximum explosion pressure, P_{max}; deflagration index, K_{St}) are measured in 20 L and/or 1 m³ vessels, according to standard procedures (ASTM E1226-19, 2019; BS EN 14034-1, 2004). To assess dusts deflagration parameters in the 20 L vessel that can be correlated to those from the 1 m³ vessel, calibration and procedures are standardised by properly setting the ignition delay time (i.e., the initial turbulence level). According to the standard procedures, measurements of deflagration index in the 20 L and in the 1 m³ vessel provide the same results if the ignition delay time is properly chosen as equal to (60 ±5) ms in the 20 L vessel and equal to (600 ± 100) ms in the 1 m³ vessel (ASTM E1226-19, 2019; BS EN 14034-1, 2004). Nevertheless, when testing dusts different from the reference ones (e.g., lycopodium), many discrepancies may be found (Clouthier et al., 2019; Proust et al., 2007; Taveau et al., 2019). Di Benedetto et al. (2013) have shown that within the 20 L sphere, it is not possible to generate uniform dust dispersion and turbulence (Di Benedetto et al., 2013). In particular, the turbulence level and the dust particle

distribution inside the 20 L sphere significantly depend on dust size, concentration, shape and density (Di Benedetto et al., 2010; Di Sarli et al., 2013; Di Sarli et al., 2014; Russo et al., 2013; Portarapillo et al., 2020a). In a recent work, we developed and validated a CFD model able to get insights into the fluid flow which is established inside the 1 m^3 vessel, when injecting either dust-free air or dust-air mixtures, and to visualize the dust dispersion process (Portarapillo et al., 2020b). Results showed that in both vessels, the dust is mainly concentrated in the outer zones of the vortices generated inside the container, so the dust concentration is not uniform (Portarapillo et al., 2020b). Conversely, the turbulent kinetic energy maps showed that the spatial distribution of the turbulent kinetic energy is quite uniform in the 1 m^3 vessel and much lower than the one found in the 20 L vessel. This should result in a better control of the initial level of turbulence and its lower dependence on dust properties. In this work, we aim at extending our model to simulate the effect of dust size on the dust dispersion, turbulence level and theoretical deflagration index evaluation inside the 1 m^3 vessel.

2. Model description

Model details of dust dispersion in the 1 m^3 vessel equipped with the perforated annular nozzle are given elsewhere (Portarapillo et al., 2020b). Briefly, the fluid flow equations (i.e., time-averaged Navier-Stokes) were discretized using a finite-volume formulation on the three-dimensional unstructured grid (478449 elements) and solved by using the standard k-ε turbulence sub-model. The flow of the solid phase was solved with the Lagrangian formulation using the Discrete Phase Model (DPM). The particle-fluid interaction is of two-way coupling type. First-order time integration was used to discretize temporal derivatives with a time step of $4 \cdot 10^{-5}$ s. For the sake of comparison, CFD simulations were carried out with a previously developed and validated model of dust dispersion in 20 L sphere equipped with rebound nozzle (Di Benedetto et al., 2013). The rebound nozzle is an alternative to the perforated annular one for the formation of the dust cloud (ASTM E1226-19, 2019). Both nozzles are present in standard test description and should generate a uniform dust cloud within the spherical vessel. Actually, previous studies have shown that both dispersion systems have important issues and differences in the dust feed in the sphere, dust concentration distribution and turbulence level and control (Di Sarli et al., 2015). Computations were performed for both the vessels for a dust with density equal to 2046 kg/m^3 and variable diameter (200 and 400 μm), using Ansys Fluent (release 2019R2). The simulation conditions for both standard vessels are summarized in Table 1.

Table 1: Simulation conditions

Parameter	1 m^3	20 L
Initial pressure of container (bar)	21	21
Initial pressure of sphere and container (bar)	1	0.4
Dust concentration (g/m^3)	100	100
Dust density (kg/m^3)	2046	2046
Dust diameter (μm)	200; 400	200; 400
Time step (s)	$4 \cdot 10^{-5}$	$1 \cdot 10^{-4}$
Number of time steps	15000	600

3. Results

Figure 1 shows the time sequence of the turbulent kinetic energy maps as computed over the frontal (x-z) plane in case of dust-free air (a) and dust-air mixtures with concentration 100 g/m^3 and dust diameters of 200 μm (b) and 400 μm (c) in the 1 m^3 vessel. The maps of dust-free air turbulence level are symmetric while the maps obtained in the presence of dust are non-symmetric due to the dust entrainment by the fluid flow. The results showed that the presence of particles in the flow has a significant effect on all the flow variables. Most notably, the distribution of all the parameters becomes asymmetric, because of the gravitational effect on the particles and particle sedimentation (Kartushinsky et al., 2011). In the case of dust size equal to 400 μm, at 600 ms, the flow field is more similar to that of dust-free air, likely due to the occurrence of a strong sedimentation phenomenon.

In order to better visualise the preferential paths of the dust, we mapped the particle tracks. The spatial-temporal distribution of dust concentration inside the sphere is represented through the ratio (χ) between the dust concentration and the nominal dust concentration (C = 100 g/m^3) in the 1 m^3 vessel. In Figure 2 and Figure 3, the time sequence of the particle tracks coloured by χ is shown as obtained on the (x-z) plane (a) and in the whole sphere (b) oriented as in the empty image in the case of dust at 200 μm and 400 μm, respectively. In the case of 200 μm (Figure 2), starting from 400 ms, the dust creates a three-dimensional cross inside the vessel due to the dust dispersion system and the formation of turbulence macro-vortices. In particular, at the ignition

time (t = 600 ms), the cloud is not uniform. In the case of 400 µm (Figure 3), the three-dimensional cross structure does not form because it becomes more difficult for the fluid flow to entrain the dust which then follows a completely different path with respect to the fluid. Therefore, also in the 1 m³ vessel, on increasing the dust diameter the preferential paths are much more evident suggesting that the dust dispersion is worst. It is worth noting that a large amount of dust is present on the sphere bottom, due to sedimentation. Moreover, a worse feeding is attained, with most of the dust trapped in the perforated annular nozzle on increasing dust diameter. Indeed, the averaged dust concentration in the 1 m³ sphere is reduced by about 10% in the case of dust with diameter of 400 µm.
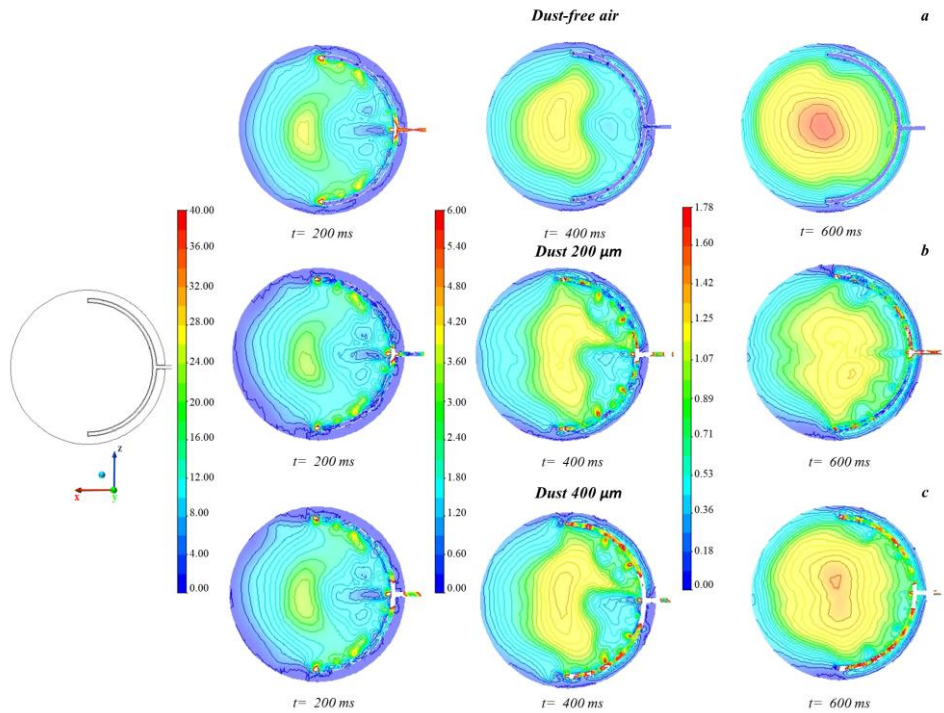
Figure 1: Time sequence of computed turbulent kinetic energy maps (m²/s²) in the 1 m³ vessel: dust-free air (a), dust at C=100 g/m³ and d=200 µm (b) and dust at C=100 g/m³ and d=400 µm (c), (x-z) plane
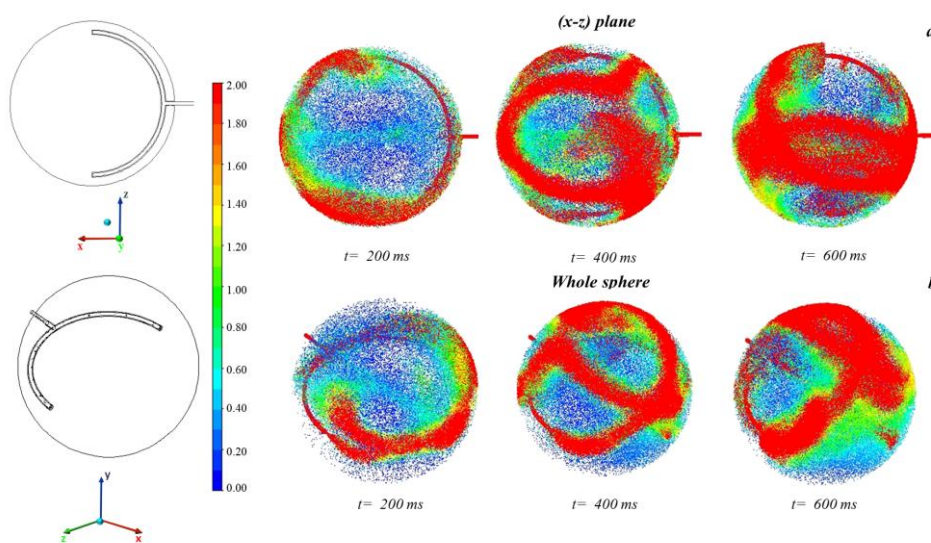

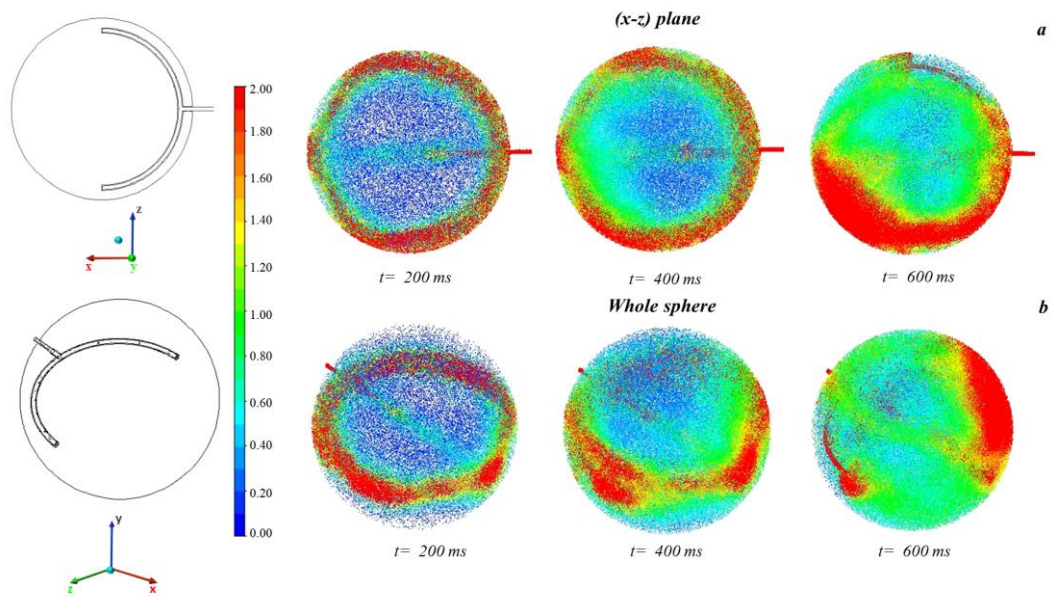Figure 2: Time sequence of particle tracks coloured by χ in the 1 m³ vessel: (x-z) plane (a) and whole sphere (b), C=100 g/m³ and d=200 µm

Figure 3: Time sequence of particle tracks coloured by χ in the 1 m³ vessel: (x-z) plane (a) and whole sphere (b), C=100 g/m³ and d=400 μm

Figure 4 shows the temporal trend of the DPM concentration as computed in the centre of the 1 m³ vessel as a function of time for dust dispersion at d=200 μm (black line) and d=400 μm (red line). At the ignition delay time (t=600 ms), the 200 μm dust shows a concentration in the centre equal to 66 g/m³ while dust at 400 μm shows a concentration equal to the nominal value, C=100g/m³. It is worth noting that in this last case, as discussed above, the quantity of dispersed dust is very low due to both the trapping in the perforated annular nozzle and the sedimentation. Indeed, the red line in Figure 4 shows a continuous increase in the concentration value, but it rapidly decays starting from 500 ms due to the sedimentation phenomenon. However, the concentration in the case of dust at 400 μm is always higher than the 200 μm case (Figure 5). In the former case, the dust leaves the perforated annular ring and, once the turbulence decays, begins to settle occupying the entire sphere and therefore also its centre. In the latter, the particles accumulate on the walls of the sphere due to the presence of macro-vortices (generated by the dust dispersion method), forming the cross structure seen in Figure 2 and leaving the internal zone at low concentration values.

Figure 6 shows the turbulent kinetic energy (m²/s²) profiles on a cut line (indicated on the left side) for 1 m³ vessel (a) and 20 L vessel (b) in the case of dust-free air (black line), and dust/air mixtures with dust size d=200 μm (red line) and d=400 μm (blue line). In both vessels, dust-free air case is characterized by the highest turbulence level. As reported in the literature, as long as the diameter is small (<100 μm), dust particles are partially entrained by the fluid flow (Di Benedetto et al., 2013). On increasing the dust diameter (e.g., d≥200 μm), it becomes more difficult for the fluid flow to entrain the dust which then follows different paths with respect to the fluid and, consequently, different turbulent kinetic energy profiles are establish (see red line in Figure 6). Further increasing the dust diameter (e.g., 400 μm), the sedimentation phenomenon becomes more severe as the turbulence dissipates, the air cannot support the dust dispersion that, once left the perforated annular nozzle, falls down leaving the velocity flow field similar to that of the dust-free air case.

To assess the effect of turbulence on the evaluation of deflagration index with the two standard vessels at 100 g/m³, we estimated the theoretical K_{St} as shown elsewhere (Portarapillo et al., 2020b). Considering only the effect of turbulence, whatever the diameter, the dust is classified always St-1 in the 1 m³ vessel. Conversely, in the 20 L vessel, starting from the most dangerous condition in which the flow field is similar to that of the dust-free air case (St-3), the classification could significantly vary according to the particles-fluid flow interaction. Therefore, given the great non-uniformity of turbulence degree, the measurement in the 20 L is more susceptible/sensitive to variations in the properties of the dust particles, reducing the repeatability/reliability of the measurements of the explosivity parameters.
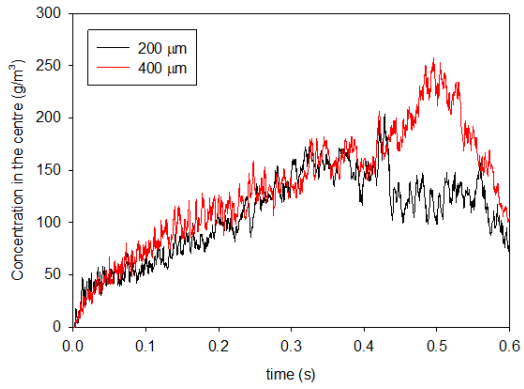
Figure 4: DPM concentration as computed in the centre of the 1 m^3 vessel as a function of time for dust dispersion at d=200 µm (black line) and d=400 µm (red line) C=100 g/m^3
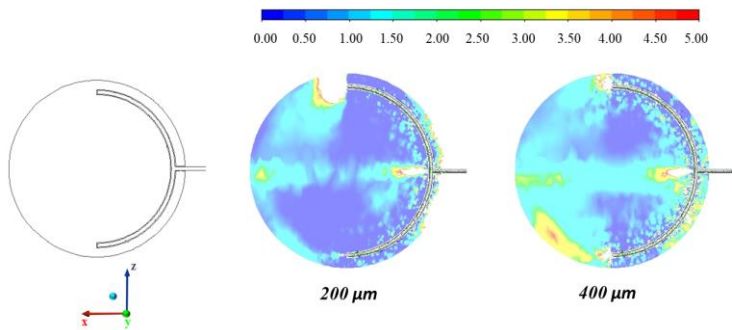

Figure 5: Computed maps of DPM concentration at 600 ms for dust dispersion at d=200 µm (left) and d=400 µm (right), (x-z) plane
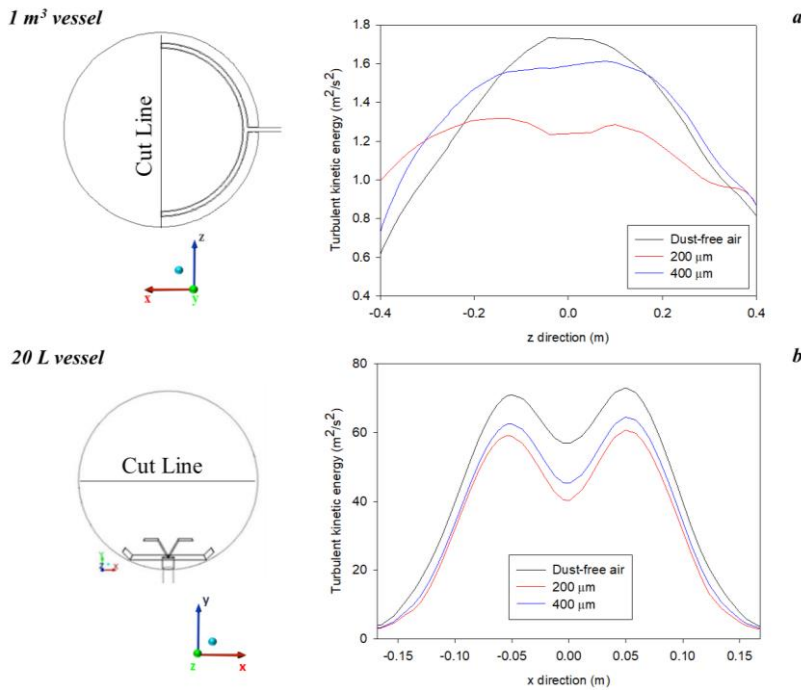

Figure 6: Turbulent kinetic energy (m^2/s^2) profiles on a cut line (indicated on the left side) for 1 m^3 vessel (a) and 20 L vessel (b): dust-free air (black line), dust dispersions at d=200 µm (red line) and d=400 µm (blue line)

4. Conclusions

CFD simulations of the dust dispersion inside the 1 m^3 standard vessel were performed at different values of the dust diameter. The time sequences of turbulent kinetic energy maps show that turbulent kinetic energy is quite uniform inside the whole vessel and in the case of 400 μm, at 600 ms the flow field is more similar to that of dust-free air, due to the occurrence of particle sedimentation and incomplete feeding. The different particles-fluid interaction obtained varying the dust diameter is further confirmed by the time sequence of particle tracks. On increasing the dust diameter, the dust and the fluid flows are independent, and the sedimentation phenomenon becomes more severe as the turbulence dissipates leaving the velocity flow field similar to that of the dust-free air case. Moreover, a worse feeding is attained, with most of the dust trapped in the perforated annular nozzle on increasing dust diameter. However, from a comparison with the 20 L vessel in terms of theoretical deflagration index assessment, given the great uniformity of turbulence degree, the 1 m^3 vessel is less susceptible and influenced by the dust intrinsic properties that influence the kind of particles-fluid flow interaction.

References

ASTM E1226-19, 2019, Standard Test Method for Explosibility of Dust Clouds, ASTM International West Conshohocken, 1–15.

BS EN 14034-1, 2004, Determination of explosion characteristics of dust clouds Part 1: Determination of maximum pressure Pmax of dust clouds 3, 1-44.

Clouthier, M.P., Taveau, J.R., Dastidar, A.G., Morrison, L.S., Zalosh, R.G., Ripley, R.C., Khan, F.I., Amyotte, P.R., 2019, Iron and aluminum powder explosibility in 20-L and 1-m3 chambers, Journal of Loss Prevention in the Process Industries, 62, 103927.

Di Benedetto, A., Russo, P., Amyotte, P., Marchand, N., 2010, Modelling the effect of particle size on dust explosions, Chemical Engineering Science, 65, 772–779.

Di Benedetto, A., Russo, P., Sanchirico, R., Di Sarli, V., 2013, CFD Simulations of Turbulent Fluid Flow and Dust Dispersion in the 20 Liter Explosion Vessel, AIChE Journal, 59, 2485–2496.

Di Sarli, V., Russo, P., Sanchirico, R., Di Benedetto, A., 2013, CFD simulations of the effect of dust diameter on the dispersion in the 20L bomb, Chemical Engineering Transactions, 31, 727–732.

Di Sarli, V., Russo, P., Sanchirico, R., Di Benedetto, A., 2014, CFD simulations of dust dispersion in the 20 L vessel: Effect of nominal dust concentration, Journal of Loss Prevention in the Process Industries, 27, 8–12.

Di Sarli, V., Sanchirico, R., Russo, P., Di Benedetto, A., 2015, CFD modeling and simulation of turbulent fluid flow and dust dispersion in the 20-L explosion vessel equipped with the perforated annular nozzle, Journal of Loss Prevention in the Process Industries, 38, 204–213.

Kartushinsky, A.I., Michaelides, E.E., Rudi, Y.A., Tisler, S. V., Shcheglov, I.N., 2011, Numerical simulation of three-dimensional gas-solid particle flow in a horizontal pipe, AIChE Journal, 57, 2977–2988.

Portarapillo, M., Di Sarli, V., Sanchirico, R., Di Benedetto, A., 2020a, CFD Simulation of the Dispersion of Binary Dust Mixtures in the 20 L Vessel, Journal of Loss Prevention in the Process Industries, 67, 104231.

Portarapillo, M., Trofa, M., Sanchirico, R., Di Benedetto, A., 2020b, CFD simulations of dust dispersion in the 1 m3 explosion vessel, Journal of Loss Prevention in the Process Industries, 68, 104274.

Proust, C., Accorsi, A., Dupont, L., 2007, Measuring the violence of dust explosions with the "20 l sphere" and with the standard "ISO 1 m3 vessel". Systematic comparison and analysis of the discrepancies, Journal of Loss Prevention in the Process Industries, 20, 599–606.

Russo, P., Amyotte, P.R., Khan, F.I., Di Benedetto, A., 2013, Modelling of the effect of size on flocculent dust explosions, Journal of Loss Prevention in the Process Industries, 26, 1634–1638.

Taveau, J.R., Lemkowitz, S.M., Hochgreb, S., Roekaerts, D.J.E.M., 2019, Metal dusts explosion hazards and protection, Chemical Engineering Transactions, 77, 7–12.